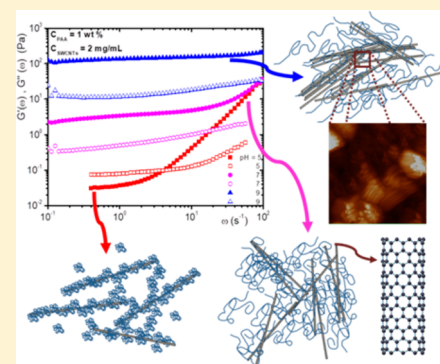


# Tuning the Viscoelastic-Gel Transition of Single-Wall Carbon Nanotubes Embedded in pH-Responsive Polyelectrolyte Solutions

Atiða Selmani,<sup>†,‡,#</sup> Antonio Tavera-Vázquez,<sup>‡,#</sup> Cristina Garza,<sup>‡</sup> and Rolando Castillo<sup>\*,‡,§</sup><sup>†</sup>Laboratory for Biocolloids and Surface Chemistry, Division of Physical Chemistry, Ruđer Bošković Institute, Bijenička cesta, 54, 10000 Zagreb, Croatia<sup>‡</sup>Instituto de Física, Universidad Nacional Autónoma de México, P.O. Box 20-364, 01000, México City, México

**ABSTRACT:** We present the detailed rheological changes that occur when small quantities of single-wall carbon nanotubes are dispersed in a poly(acrylic acid) water solution, around the overlap polymer concentration, up to the gel point. Here, pH is used to tune the gel formation. Suspensions of nanotubes at  $\text{pH} \leq 5$  are exfoliated and dispersed by the polymer. Contacts between the nanotubes are mainly through polymer entangling, and the suspension is viscoelastic. At  $\text{pH} > 5$ , the polymer is charged, and the solution is not a good solvent for the nanotubes anymore. Nanotube bundles covered with polymer are formed and mechanically percolate along the fluid until they become arrested. As a consequence, the rheological behavior is dominated by a mesoscale superstructure formed by nanotubes and polymer, where viscoelasticity is lost and the suspension becomes elastic. At  $\text{pH} \geq 9$ , the surroundings for the nanotubes are worse, bundles and flocs grow to a larger extent, and they can be observable by scanning microscopies. When the suspension becomes a critical gel, the relaxation moduli can be modeled by a power law in the frequency domain in agreement with the model developed by Winter and co-workers.



## 1. INTRODUCTION

Liquids with dispersed rodlike particles present different microstructural orderings that exhibit different rheological responses.<sup>1</sup> For applications, it is essential to foresee the rheological response of these suspensions from the underlying properties of the rods and the dispersant agent, as well as other features that affect their response as percolation, phase stability, aggregation, flexibility, polydispersity, etc. It is not uncommon that rodlike colloidal suspensions in highly viscous polymers flow at low shear stress with quiescently formed rod networks which rapidly break down and then regel upon cessation of flow. Single-wall carbon nanotubes (SWCNTs) dispersed in a polymer are a clear model example of this case. It is stated that when the rod length is such that the suspension is in the colloidal domain, four properties control the microstructure, dynamics, and rheology of rod-containing materials:<sup>1</sup> interparticle forces, aspect ratio, particle number density, and flexibility. The principal way to generate a significant level of elasticity in colloidal suspensions is to arrest particle dynamics at the microscopic level, although dynamic arrest can lead to gelation with a slow dynamics mainly due to attractive interactions and bonding, or to vitrification with a slow dynamics primarily due to excluded volume interactions and packing. However, the microstructures linked to these two kinds of slow dynamics are different,<sup>1</sup> heterogeneous fractal clusters of rods for the former and a homogeneous rod network for the latter. The volume fraction range for the transition between these two limiting cases is strongly aspect ratio-dependent.

Preparation of nanocomposites made of carbon nanotubes (CNTs) embedded in a polymer matrix could produce materials with properties that might be used for many applications, especially when the nanofiller can provide the polymer matrix with valuable functional properties, as in the case of SWCNTs that exhibit high mechanical strength, high stiffness, and good electrical conductivity.<sup>2,3</sup> Nevertheless, the poor solubility of carbon nanotubes and the fact that they are not prone to form dispersions lead to their potential applications difficult to be reached. These circumstances are a consequence of their strong van der Waals interactions that produce the formation of the large nanotube bundles. Here, the attraction is directly proportional to the diameter of the nanotubes and inversely related to the intertube distance.<sup>4</sup> Therefore, even at a modest concentration, the intertube attraction yields the formation of aggregates or bundles making this attraction the most significant challenge toward the dispersion of SWCNTs in a polymer matrix. However, some polymers have been used effectively as exfoliation agents of nanotube bundles making possible the incorporation of the nanotubes as individual entities or as very thin bundles. Many mechanisms have been mentioned for explaining why they are so effective.<sup>5,6</sup> Some examples of polymers dispersing SWCNTs can be found in the literature.<sup>7–11</sup> To improve the dispersion, CNTs can be modified non-covalently<sup>12</sup> or covalently,<sup>13–16</sup> or with the use of surfac-

Received: September 12, 2017

Revised: December 5, 2017

Published: December 6, 2017

tants,<sup>17–19</sup> DNA,<sup>20</sup> or proteins.<sup>21</sup> These chemical and physical approaches can be successful at low and intermediate CNT concentrations. Nonetheless, the dispersion of CNTs is still a challenging problem at high concentration.

The behavior of CNTs dispersed in a polymer matrix can be characterized into three regimes according to the concentration and their orientational or structural correlation.<sup>22</sup> In the dilute regime, dispersed nanotubes or completely exfoliated behave as individual tubes or as thin dispersed bundles. In this regime, short-range intertube interactions are present, but long-range interactions are negligible. The transition from dilute to semidilute regime coincides with a percolation event. As exfoliation is improved, the percolation transition occurs at a lower concentration. In the semidilute regime, the extent of exfoliation of the nanotubes, or their small bundles, and their interaction with each other control the overall rheological behavior of the nanocomposite. Close to this percolation threshold, dramatic changes in the rheological properties are observed that arise supposedly from the intertube interaction. Incorporation of CNTs in the polymer gradually transforms the liquid-like behavior to solid-like behavior where the storage ( $G'(\omega)$ ) and loss modulus ( $G''(\omega)$ ) are almost frequency independent at low frequencies and  $G'(\omega) > G''(\omega)$ .<sup>22</sup> The percolation threshold decreases with an increase in the aspect ratio of the CNTs suggesting the formation of a matrix spanning path at a low or modest nanotube loading. At concentrations significantly larger than the percolation concentration, the excluded-volume interactions lead to an isotropic–nematic transition as occurring in CNTs dispersed in acid,<sup>23</sup> where the concentrated regime starts and the rheological properties tend to reach asymptotic values. More about the rheological behavior of CNTs in a polymer matrix can be found elsewhere.<sup>22</sup>

Polar solvents can dissociate polymers with ionizable groups leaving charges on the polymer chains and releasing counterions into the solution.<sup>24</sup> Electrostatic interactions between charges in the polymer lead to a rich behavior different from those of uncharged polymers. Some polyelectrolytes are also stimuli-responsive polymers that show significant reversible structural changes in response to small changes in their environment, such as pH.<sup>25</sup> One example is the poly(acrylic acid) (PAA).<sup>26</sup> The carboxyl groups of polyacrylic polymers in aqueous solution are protonated at low pH and neutrally charged; thus, hydrophobic interactions promote a relatively compact polymer structure. Electrostatic repulsion between some charged, not protonated carboxyl groups, leads to the formation of extended polymer structures; a sort of loose coil. This pH-responsive conformational change just occurs in relatively high molar mass PAA (>16.5 kDa).<sup>26</sup> PAA is protonated in an aqueous medium at pH < 3, as the pH increases, carboxylic groups are deprotonated, forming a polyelectrolyte that becomes highly charged (pH ~ 5), and its backbone becomes stretched, forming a 3D interacting network of polymer chains. As a consequence, the size of the PAA and the regular polymer–polymer interactions both lead to a significant change in the rheological behavior of this polymer in water solution with different  $[H^+]$  content.

There is not too much literature available focusing on the dilute regime rheology of CNTs dispersed in a polymer matrix, probably because the viscoelastic response of the polymer would far exceed that of the dispersed CNTs. However, as mentioned above at the percolation concentration, a matrix spanning network must be formed leading to increasing elasticity because the CNTs are arrested. Around this percolation concentration, the rheological behavior must be dominated by that mesoscale

superstructure. Here, we will present the rheological behavior of dilute suspensions of SWCNTs in a polyelectrolyte matrix which possesses an extra degree of freedom; the polymer is sensitive to pH. First, we will determine how pH controls the rheological behavior of the PAA polyelectrolyte at different polymer concentrations. Although this rheological behavior is not entirely unknown, it depends on the degree of polymerization. Therefore, we will obtain this behavior for our specific case in a way that will be useful for the second part of this study, where we add SWCNTs to a dilute polymer matrix. In this case, we find out that pH strongly impacts the rheological properties of these composites. The central question to answer in this report will be why the rheological behavior of PAA/water solutions at different pH values is so strongly modified, around the overlap concentration, when small quantities of SWCNTs are added to this liquid mixture. As we will see, the rheological behavior is dominated by the mesoscale superstructure at concentrations close to the percolation threshold at high pH, where some of its fingerprints are observable with scanning microscopies. This structure behaves as a critical gel described in physical and chemical gelation considered by Chambon and Winter,<sup>27</sup> which would be in agreement with the assumption that the dynamic arrest that leads to gelation in our case is mainly due to attractive interactions between SWCNTs. We will model the rheological behavior of the SWCNTs/PAA water suspensions using the method developed for describing these physical critical gels.<sup>28</sup> This study allows us to get some physical insight of what is happening in the suspension close to the gel point.

## 2. EXPERIMENTAL SECTION

**2.1. Materials.** Polyacrylic acid (PAA,  $M_w = 450,000$  g mol<sup>-1</sup>, Sigma-Aldrich, USA) was used as received. NaOH ( $\geq 98\%$ ) is from Sigma-Aldrich (Sweden), HNO<sub>3</sub> (68%) and HCl (36%) solutions are from J. T. Baker (USA). All solutions were prepared with nanopure water (Nanopure-UV, USA; resistivity  $\sim 18$  M $\Omega$  cm). Standard buffers (pH = 4, 7, and 10) from J. T. Baker (Mexico) were used for electrode calibrations. The single-wall carbon nanotubes (SWCNTs) were purchased from Nano-C Inc. (85–90%, Nano-CPT-100, length  $\approx 1$   $\mu$ m and diameter  $\approx 1$  nm, USA) manufactured via combustion method. They contain iron as well as amorphous carbon impurities, so they needed a further purification. We followed this procedure: 300 mg of SWCNTs were suspended in 300 mL of 3 M HNO<sub>3</sub>, stirred with a magnetic stirrer, and sonicated for 10 min using a standard bath sonicator (Cole-Parmer, USA) to disperse large agglomerates and to obtain a homogeneous suspension. This suspension was refluxed for 48 h at 125 °C under magnetic stirring, and then it was neutralized with 3 M NaOH. The resulting precipitates were filtered and extensively washed with water until the pH was close to the values of the nanopure water (pH  $\approx 6.5$ ) to eliminate remnants of NaNO<sub>3</sub> and NaOH coming from the purification process. The SWCNTs were dried at 80 °C for 6 h in air and stored in glass bottles.

**2.2. Sample Preparation.** PAA solutions with a different weight fraction (1–6 wt %) were prepared by dissolving dry PAA powder in water under magnetic stirring at 40 °C. The pH of the PAA solutions (pH = 3, 5, 7 and 9) was adjusted with HCl and NaOH both at 1 M. pH was measured with a pH-meter (Cole-Parmer, USA) equipped with a combined glass electrode (Cole-Parmer, USA) previously calibrated with standard buffers. The polymer solutions were left under magnetic stirring for 24 h to reach equilibrium. A buffer to stabilize suspension pH was not

used in these experiments to avoid screening of the polyacid charges by co-ions.

The SWCNTs suspensions were prepared by suspending purified dry SWCNTs powder in a PAA water solution at a specific weight fraction with the pH previously adjusted (pH = 5, 7, and 9). The concentrations for SWCNTs were  $C_{\text{SWCNTs}} = 0.5, 1, \text{ and } 2 \text{ mg/mL}$ , and for PAA:  $C_{\text{PAA}} = 1\text{--}6 \text{ wt } \%$ . The SWCNTs suspensions were ultrasonicated (43 kHz, QSonica, USA) at 50 W for 3 h with time cycles, 30 s on and 30 s off, in a water–ice bath to prevent heating of the samples leading to SWCNTs breakage.

**2.3. Atomic Force Microscopy.** The SWCNTs/PAA suspensions were prepared at two different concentrations,  $C_{\text{SWCNTs}} = 0.01 \text{ and } 0.02 \text{ mg/mL}$  at three different pH values (5, 7 and 9).  $10 \mu\text{L}$  of these samples were deposited via spin coating onto freshly cleaved mica substrates and then centrifuged at 6000 rpm. The dried specimens were surveyed with a scanning probe microscope (JSTM-4200, JEOL Ltd., Japan) with an  $80 \times 80 \mu\text{m}$  scanner. To obtain topographic images of the samples, we used the noncontact mode with silicon cantilevers (typical force constant of 46 N/m and a tip radius of  $\sim 10 \text{ nm}$ , Mickromash, USA).

**2.4. Electron Microscopy.** We used a transmission electron microscope (TEM; JEM-1200EX11, JEOL, Japan) working at 100 kV, and an extreme-resolution analytical field-emission scanning electron microscope (SEM; JSM-7800F JEOL Ltd. Japan) working at low electron acceleration voltages.<sup>29</sup>

A few microliters drop of SWCNTs/PAA suspension was deposited on a standard copper TEM grid with a carbon covered collodion layer. The excess of sample deposited on the grid was absorbed with paper and dried at ambient conditions to be observed with TEM. In the case of the SEM samples, previous to its introduction in the microscope, the samples were covered with a thin carbon layer to ensure that the sample on the grid is conductive. The low energy incident electrons on a specimen produce secondary electrons due to the emission of valence electrons of the constituent atoms, at the top surface of the sample. These emitted electrons form standard topography images using the lower electron detector (LED), or high-resolution topography images using the upper electron detector (UED).

**2.5. UV–Vis Measurements.** UV–vis measurements were performed with an Evolution 300 UV–vis spectrometer (Thermo Fisher Scientific, USA) in the 200–600 nm wavelength range. UV–vis experiments were performed for samples with  $C_{\text{SWCNTs}} = 0.02 \text{ mg/mL}$  and pH = 5, 7, and 9. In all cases,  $C_{\text{PAA}} = 2 \text{ wt } \%$ .

**2.6. Rheology Measurements.** Rheological measurements were carried out in a Kinexus ultra + rheometer (Malvern Instruments, USA). Experiments were done using a cone–plate geometry ( $4^\circ$ , diam., 40 mm) at  $20^\circ\text{C}$ . The PAA solutions and SWCNTs/PAA suspensions were allowed to relax at rest for 2 days prior to the measurements. Flow curves and oscillatory measurements were developed. In the latter, the angular frequency range was from  $10^{-1}$  to  $5 \times 10^2 \text{ s}^{-1}$ . The strain was 25% for the PAA solutions and 5% for the SWCNTs–PAA suspensions to ensure a linear deformation.

### 3. RESULTS AND DISCUSSION

First, we will present how pH controls the rheological behavior of the PAA solutions at different concentrations for the specific degree of polymerization used here. Next, we will present the

results when small quantities of SWCNTs are added to the PAA solutions.

**3.1. Rheological Behavior of the PAA.** In the 450 kDa PAA solution, a significant fraction of the carboxyls is ionized at high dilution and above its isoelectric point.<sup>26</sup> Intramolecular segments repel each other so that the macromolecule can adopt a loose conformation. The conformational transition driven by the state of ionization of the carboxylic groups is reversible from a relatively globular shape to a fully solvated open coil conformation around  $\text{pH} \sim 4.5$ ;<sup>26</sup> this value depends on the degree of polymerization. Thus, the rheological properties of the solution are influenced by pH.

**3.1.1. Viscosity.** Figure 1 presents the apparent viscosity,  $\eta$ , vs the shear rate,  $\dot{\gamma}$ , curves for the polyelectrolyte solutions at low

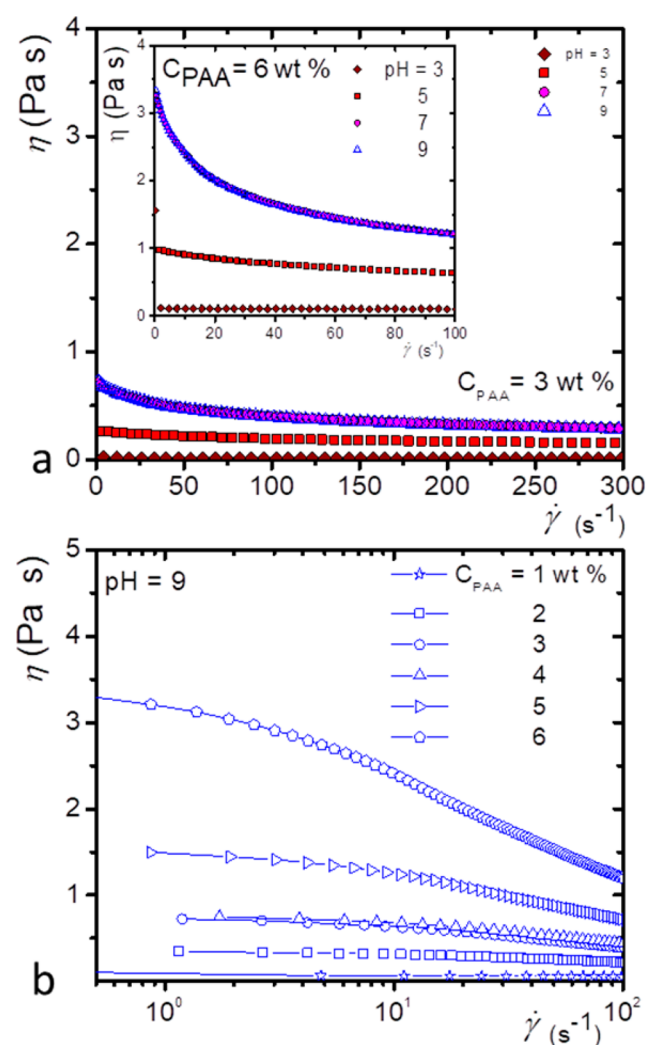


**Figure 1.** Apparent viscosity for the polyelectrolyte solutions at different pH and polymer concentration. (a)  $\eta$  vs  $\dot{\gamma}$  at constant concentration ( $C_{\text{PAA}} = 3 \text{ wt } \%$ ); inset,  $C_{\text{PAA}} = 6 \text{ wt } \%$ ; (b)  $\eta$  vs  $\dot{\gamma}$  for different  $C_{\text{PAA}}$  at constant pH.

concentration and different pH values. These curves are determined by steadily increasing the shear rate. In all cases, the solutions shear thin. Thixotropic loops do not present hysteresis (not shown). In general, the viscosity is small and increases with pH at a fixed concentration, (Figure 1a for 3 wt % and 6 wt %). The curves with the lowest values that we measured correspond to  $C_{\text{PAA}} = 1 \text{ wt } \%$ ; here,  $\eta \sim 0.2 \text{ Pa s}$  at low  $\dot{\gamma}$  and pH =

9 (not shown). For a fixed pH, viscosity increases with the polymer concentration (Figure 1b). In dilute solutions, the contribution from different coils is additive, and solution viscosity increases nearly linear with polymer concentration above the solvent viscosity, and after some concentration, viscosity increases nonlinearly.<sup>30</sup> The behavior of the polyelectrolyte of interest here is consistent with previous studies developed for polyelectrolytes.<sup>25,26</sup> At high pH, the polymer has a more extended structure that promotes entangling, which also increases as the polyelectrolyte concentration increases. When the system is sheared, the flow forces the polymer to align, dropping the energy dissipation, and as a consequence viscosity decays. This is apparently the reason for shear thinning as pH and polymer concentration increase.

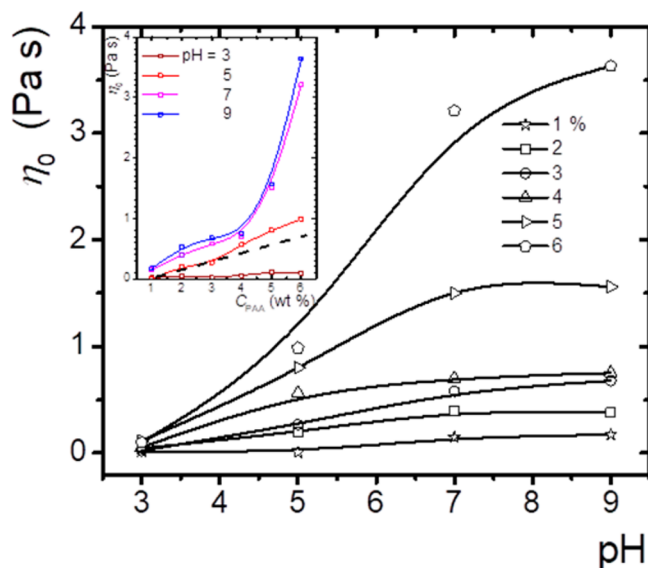


**Figure 2.**  $\eta_0$  vs pH for different polymer concentrations. Lines are a guide to the eye. Inset:  $\eta_0$  vs  $C_{\text{PAA}}$  at various pH values. The black dash line at pH = 5 shows where  $\eta_0$  is no longer linearly dependent on  $C_{\text{PAA}}$ .

Figure 2 presents  $\eta_0 = \lim_{\dot{\gamma} \rightarrow 0} \eta(\dot{\gamma})$  as a function of pH for different polymer concentrations.  $\eta_0$  increases significantly from low values, close to the solvent viscosity, up to more than 3 orders of magnitude when pH is high (7–9), and when the polymer concentration is above 4 wt %. The inset of Figure 2 presents  $\eta_0$  vs  $C_{\text{PAA}}$  at different pH values, here it is easier to observe that above pH = 5 and at  $C_{\text{PAA}} \sim 4$  wt % there is a change of behavior. Below this concentration, the interaction between polymer molecules is not significant as in the dilute regime, that is, the viscosity is low and relatively close to the solvent viscosity. After this concentration, viscosity increases drastically as in the semidilute regime because polymer molecules begin to entangle with each other. Our estimate for the overlap concentration is  $C^* \sim 4$  wt % for  $\text{pH} \geq 5$ .

**3.1.2. Viscoelastic Spectra.** The shear modulus,  $G(t)$ , exhibits a significant time or frequency dependence observed in the complex modulus  $G^*(\omega) = G'(\omega) + iG''(\omega)$ ;  $G^*(\omega) = i\omega \int_0^\infty G(t) e^{-i\omega t} dt$ . The real part is the storage, or elastic, modulus in phase with the applied shear strain. The imaginary part is the viscous, or loss, modulus that is in phase with  $\dot{\gamma}$ . Figure 3 presents some examples of the viscoelastic spectra of PAA

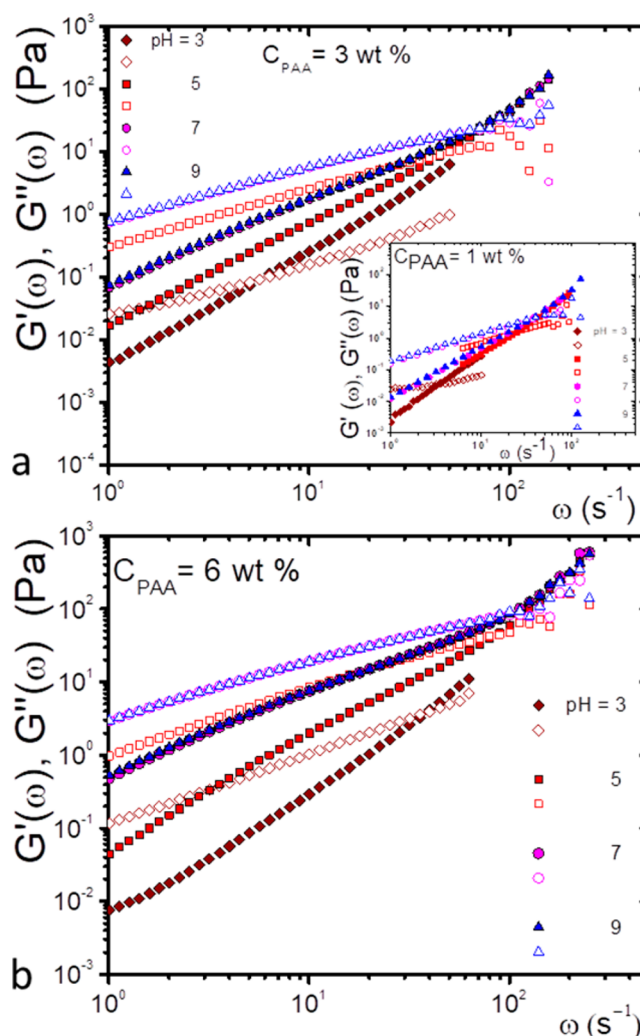


**Figure 3.** Viscoelastic spectra of PAA solutions for different values of concentrations and pH: (a)  $C_{\text{PAA}} = 3$  wt %; inset,  $C_{\text{PAA}} = 1$  wt %; and (b)  $C_{\text{PAA}} = 6$  wt %. Closed symbols,  $G'(\omega)$ ; open symbols,  $G''(\omega)$ .

solutions for different concentrations and pH. In general, the solutions are more viscous at low frequencies, and after the crossing point, ( $G_0$ ,  $\omega_0$ ) they are more elastic, as in a typical viscoelastic fluid. Both moduli increase as pH increases, at a constant  $C_{\text{PAA}}$  as illustrated in Figure 3 for pH = 3, 5, 7, and 9. The increment between pH = 3 and pH = 5 can reach an order of magnitude, but this increment decreases between higher pH values. Figure 4a presents the variation of  $G'(\omega)$  and  $G''(\omega)$  as a function of  $C_{\text{PAA}}$ , at fixed pH = 9. As the concentration increases, both curves move upward to larger moduli values. The whole behavior of the viscoelastic spectra can be summarized in Figure 4b, where  $G_0$  vs  $\omega_0$  is plotted for the PAA solutions measured at different pH and concentrations. All the crossing points collapse in a single exponential curve. For solutions with a low  $C_{\text{PAA}}$  or low pH, we find their corresponding crossing points in the lower part of the curve, as  $C_{\text{PAA}}$  or pH increase they move upward along the exponential locus. Surely, this relation between  $G_0$  and  $\omega_0$  is far from being an accident and deserves more research to understand its physical origin.

**3.2. Mesoscale Structure of SWCNTs/PAA Suspensions.** Structure and rheology behavior are intimately related. First, we will determine how the microstructure of the PAA polyelectrolyte is affected by the addition of SWCNTs at different pH

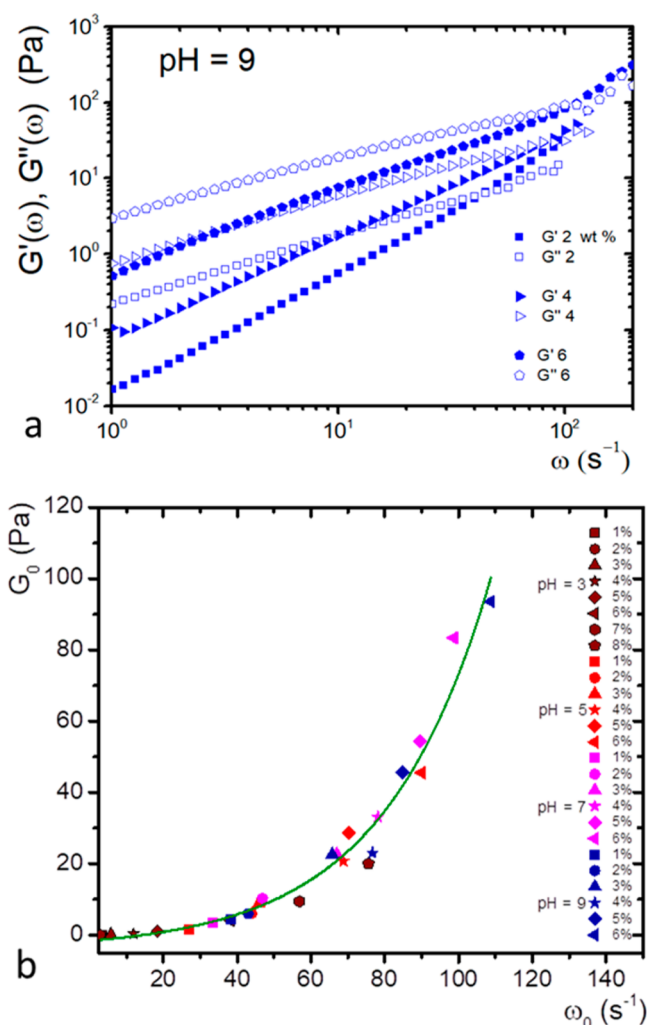


**Figure 4.** Viscoelastic spectra of PAA. (a)  $G'(\omega)$  and  $G''(\omega)$  as a function of the polyelectrolyte concentration, at constant pH = 9; Closed symbols,  $G'(\omega)$ ; open symbols,  $G''(\omega)$ . (b) The relation between  $G_0$  vs  $\omega_0$  defined by the crossing points as a function of pH and concentration. Green line, exponential fitting for all the crossing points.

values, performing UV–vis, SEM, TEM, and AFM experiments. From these experiments, we will show that the SWCNTs are less exfoliated in suspensions at pH = 9, and apparently, they are forming bundles entangled with PAA molecules. Therefore, the rheological behavior of this system will be dominated by the mesoscale superstructure at concentrations close to the mechanical percolation threshold at high pH.

**3.2.1. UV–Vis Spectra.** UV–vis has been used to determine the degree of exfoliation of the SWCNTs in a polymer matrix.<sup>7,31</sup> An absorbance increment corresponds to exfoliation of the SWCNTs bundles in the suspension. Bundles are transformed by the action of a dispersant agent from thick bundles to thin bundles or single nanotubes. UV–vis experiments were carried out to determine the effect of pH on the degree of exfoliation of SWCNTs in our suspensions, and they will be a useful piece of information to understand the rheological behavior of the suspensions. Figure 5 presents our UV–vis measurements for the SWCNTs/PAA suspensions at three different pH values that are similar to those obtained for PAA in ref 7. They reveal that the SWCNTs are more exfoliated at pH = 5 in comparison to pH = 7 and pH = 9. As we increase pH, the degree of exfoliation decays; visual inspection also confirmed the formation of tiny clusters.

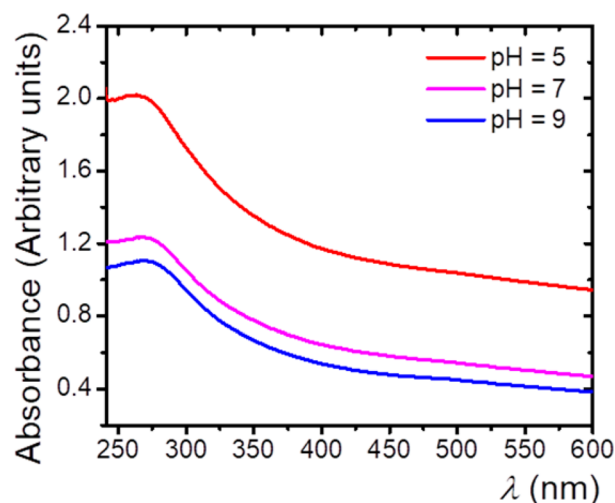


**Figure 5.** UV–vis spectra of SWCNTs/PAA suspensions at different pH values.  $C_{\text{SWCNTs}} = 0.02$  mg/mL and  $C_{\text{PAA}} = 2$  wt %.

This behavior is similar to the case when SWCNTs are exfoliated in water dispersions, using sodium dodecyl sulfate (SDS) as a dispersing agent.<sup>32</sup> Although there is no standard to determine analytically how many exfoliated SWCNTs are in a polymer dispersion to generate a calibration curve (absorbance vs concentration of exfoliated SWCNTs @  $\lambda = 280$  nm),<sup>33</sup> at high dilution, with most of the CNTs exfoliated, we estimated that the number of exfoliated SWCNTs at pH = 5 is around twice those at pH = 9. Previous reports indicate as pH increases, the mechanical percolation point is found first, and at a higher pH the electrical percolation point is reached.<sup>31</sup>

**3.2.2. Electron Microscopy (TEM and SEM).** Figure 6a presents a high voltage 100 kV-TEM image of a suspension sample ( $C_{\text{SWCNTs}} = 0.05$  mg/mL,  $C_{\text{PAA}} = 1$  wt %, pH = 9) where entangled SWCNTs are observed inside the polymer matrix. Here, all planes of the sample are projected on the 2D image since electrons are traversing the whole sample thickness. In this image, we observe SWCNTs forming thick bundles although their concentration is relatively low. In general, a secondary electron SEM image (LED) of specimens made of SWCNTs (0.02 mg/mL)/PAA (2 wt %) presents a uniform flat surface covered with globules with elongated protrusions without an apparent structure (not shown). However, with the use of high-resolution low voltage (3 kV) SEM secondary electrons (UED) in samples at pH = 9, the polymer and the SWCNTs seem to interact to form thick rods (length of several micrometers and diameter of  $\sim 0.5$   $\mu\text{m}$ ) or surfaces that wind themselves up as shown in Figure 6b–d; this does not occur in specimens at low pH. We note that these structures last long enough to be observed, notwithstanding the samples were vacuum-dried for inspection in the electron microscopes.

**3.2.3. Atomic Force Microscopy.** At low pH values ( $\leq 7$ ), topographic images do not reveal any structure (not shown), we observe just irregular globular domains over a relatively flat surface. At pH = 9, our observations changed dramatically. Figure 7 is a set of amplifications of the same area in the inspected specimen. Figure 7a presents a  $50 \times 50$   $\mu\text{m}$  topographic image where linearly oriented bead chains are easily observed. In a further amplification (Figure 7b,  $15 \mu\text{m} \times 15 \mu\text{m}$ ) we observe that the beads forming the chain have a diameter of  $\sim 0.5$   $\mu\text{m}$  and they seem to have some structure that is revealed in Figure 7c ( $2 \mu\text{m} \times 2 \mu\text{m}$ ). Here, the beads apparently are formed by stacks of

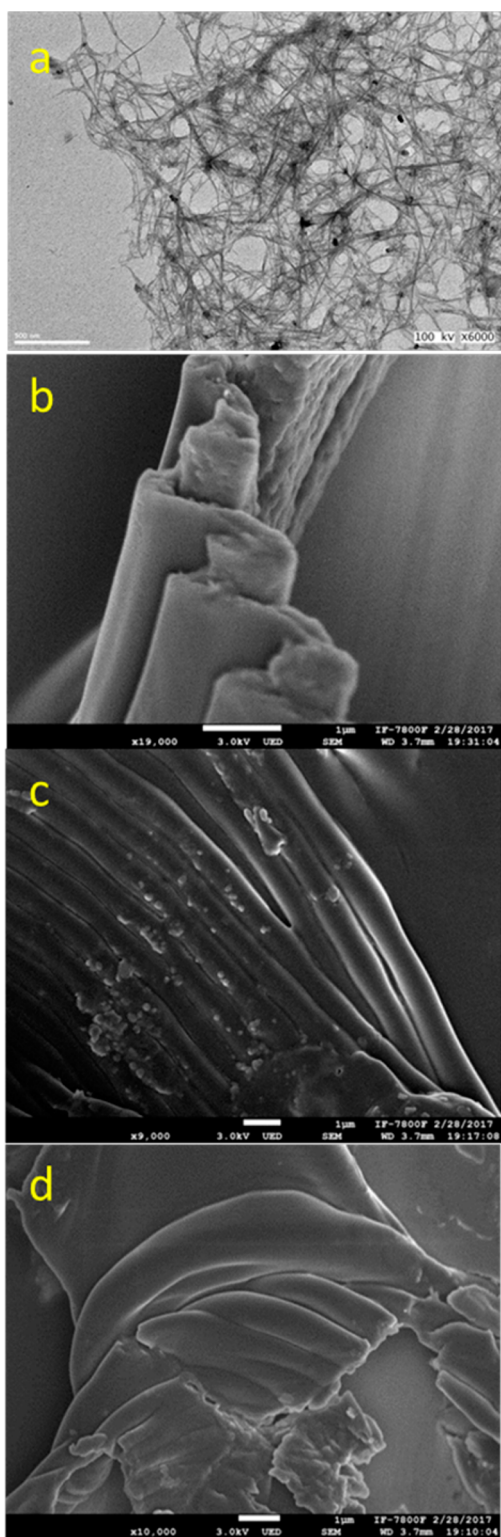


**Figure 6.** Electron microscopy images of SWCNTs/PAA suspensions. (a) TEM image:  $C_{\text{SWCNTs}} = 0.05$  mg/mL,  $C_{\text{PAA}} = 1$  wt % at pH = 9, scale bar =  $0.5 \mu\text{m}$ . (b–d) High-resolution secondary electron SEM images (UED):  $C_{\text{SWCNTs}} = 0.02$  mg/mL,  $C_{\text{PAA}} = 2$  wt %, at pH = 9; scale bars =  $1 \mu\text{m}$ .

rods, where these stacks are not all following the same direction. A further amplification shows the rods in a  $0.8 \mu\text{m} \times 0.8 \mu\text{m}$  image, Figure 7d. The thickness of these rods is in the range of

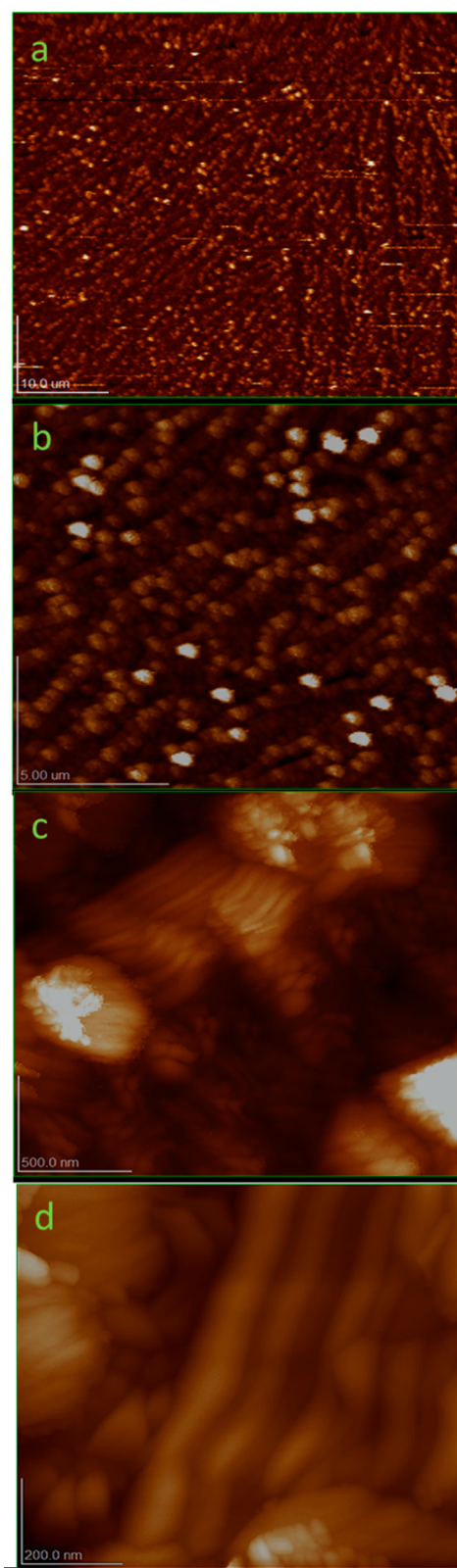


**Figure 7.** Topographic images at successive different amplifications with AFM of a specimen of  $C_{\text{SWCNTs}} = 0.01$  mg/mL dispersed in  $C_{\text{PAA}} = 2$  wt % at pH = 9. Scale bars: (a)  $10 \mu\text{m}$ , (b)  $5 \mu\text{m}$ , (c)  $0.5 \mu\text{m}$ , and (d)  $0.2 \mu\text{m}$ .

$50\text{--}70$  nm and the length is difficult to observe because the rods overlap with other stacks, but they are larger than  $0.8 \mu\text{m}$ .

**3.3. Rheological Behavior of the SWCNTs/PAA Suspensions.** 3.3.1. *Viscosity.* Figure 8 presents how the flow

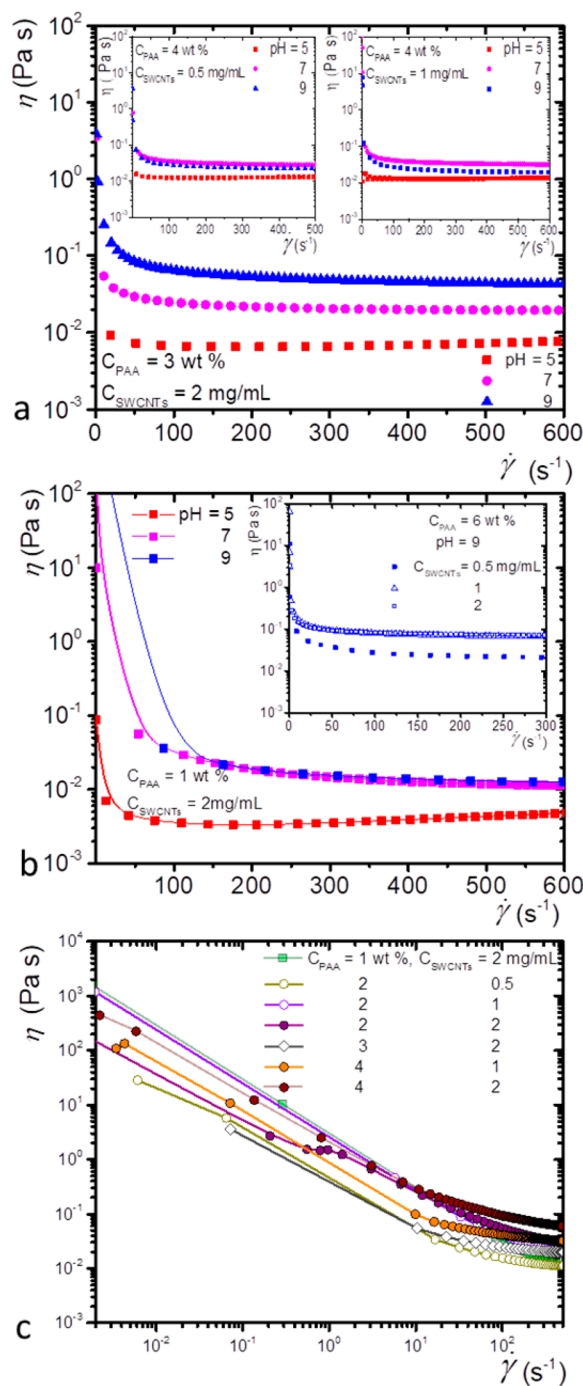


**Figure 8.** Apparent viscosity of the polyelectrolyte solutions at different pH values (5, 7, and 9) where small quantities of SWCNTs have been added. (a)  $\eta$  vs  $\dot{\gamma}$  for a suspension with  $C_{PAA} = 3$  wt % and  $C_{SWCNTs} = 2$  mg/mL. Insets  $\eta$  vs  $\dot{\gamma}$  for  $C_{PAA} = 4$  wt % and  $C_{SWCNTs} = 0.5$  (left inset), and for  $C_{PAA} = 4$  wt %, and  $C_{SWCNTs} = 1$  mg/mL (right inset). (b)  $\eta$  vs  $\dot{\gamma}$  for a suspension with  $C_{PAA} = 1$  wt % and  $C_{SWCNTs} = 2$  mg/mL. Inset  $\eta$  vs  $\dot{\gamma}$  for varying  $C_{SWCNTs}$  at constant  $C_{PAA} = 6$  wt % and pH = 9. (c) Viscosity at low  $\dot{\gamma}$  for some typical examples at pH = 7. Lines are a guide to the eye.

curves,  $\eta$  vs  $\dot{\gamma}$ , are modified varying the quantity of SWCNTs added to the liquid mixtures, at different pH values. All curves were determined by steadily increasing the shear rate. In all the cases, the suspensions shear thin and thixotropic loops do not show hysteresis (not shown). At high shear rates ( $\dot{\gamma} \geq 100$   $s^{-1}$ ), the viscosity of the suspensions is even smaller than those for the pure polymer solutions (Figure 1a), as observed in Figure 8a for

$C_{PAA} = 3$  wt % and  $C_{SWCNTs} = 2$  mg/mL or its insets. This behavior can be observed even at the lowest concentrations of CNTs ( $C_{PAA} = 3$  wt % and  $C_{SWCNTs} = 0.5$  mg/mL, not shown). In some cases, there are more than 2 orders of magnitude difference. When the system is highly sheared, in addition to the polymer alignment, the flow also tends to align rod-shaped colloids along the fluid flow direction dropping, even more, the energy dissipation as in paranematic phases;<sup>34</sup> as a consequence, viscosity decays dramatically. The addition of SWCNTs introduces a significant interaction between the polymer and the SWCNTs, despite the polymer molecules being far enough to prevent their interaction as in  $C_{PAA} = 3$  wt %; the pure polymer solution is below its  $C^*$ . In general, the apparent viscosity increases as pH increases at fixed  $C_{PAA}$  and  $C_{SWCNTs}$  (Figure 8a, its inset, and Figure 8b), although at large  $\dot{\gamma}$ ,  $\eta$  is slightly larger at pH = 7 than at pH = 9 or they are approximately equal. The inset of Figure 8b shows how the viscosity increases with the addition of CNTs for  $C_{PAA} = 6$  wt % and pH = 9. At low  $\dot{\gamma}$ , the suspensions present a dramatic change in the value of the viscosity for pH = 7 and pH = 9. Viscosity increases several orders of magnitude ( $\sim 3$ – $4$ ) with respect to its value at large  $\dot{\gamma}$ , as shown in Figure 8c for some typical examples for pH = 7; for pH = 5 the viscosity increases, but in the range of 1 order of magnitude (not shown). This seems that the system forms a structure when it is quiescent that does not resist deformation.

**3.3.2. Viscoelastic Spectra of SWCNTs/PAA Water Suspensions.** Figure 9 presents measured viscoelastic spectra of SWCNTs/PAA suspensions for different concentrations in both components and pH. At  $C_{PAA} = 1$  wt % and  $C_{SWCNTs} = 1$  mg/mL, the suspensions are still viscoelastic (Figure 9a).  $G_0$  and  $\omega_0$  both increase as the pH increases, but they are smaller, even at these low concentrations than those corresponding to the pure polymer solution (see inset Figure 3a). In the inset of Figure 9a, we observe a significant change in the rheological behavior at pH = 7 and pH = 9, when more SWCNTs are added to the suspension ( $C_{SWCNTs} = 2$  mg/mL). The crossing point disappears,  $G'(\omega) > G''(\omega)$  for approximately three decades of  $\omega$ , with a ratio between them of  $\sim 10$ , and the elastic modulus remains essentially constant at low frequencies. Therefore, the suspension behaves like a solid gel.<sup>35</sup> The same loss of viscoelasticity occurs at other low polymer concentrations, as in the case of  $C_{PAA} = 3$  wt %, with  $C_{SWCNTs} = 0.5$  mg/mL or  $C_{SWCNTs} = 2$  mg/mL presented in Figure 9b and its inset, respectively. In this case, a less amount of added nanotubes is needed to lose the crossing point; at least  $C_{SWCNTs} = 0.5$  mg/mL is enough. However, in all the cases of Figure 9, at pH = 5, the suspensions are still viscoelastic. There is a change in order of the moduli curves as can be noted in Figure 9b. In this case, the spectra at pH = 7 present larger values of  $G'(\omega)$  and  $G''(\omega)$  than those corresponding to pH = 9.

At  $C_{PAA} = 4$  wt % with a small (Figure 10a) or a large (inset of Figure 10a)  $C_{SWCNTs}$ , the moduli for pH = 7 and pH = 9 goes back to the standard order (curves at pH = 9  $\geq$  pH = 7); in this case there is no cross points either. Here, at pH = 5, below the crossover, both  $G'(\omega)$  and  $G''(\omega)$  approximately coincide. Figure 10b presents an example of how the moduli vary as  $C_{SWCNTs}$  increases at fixed pH = 7 and  $C_{PAA} = 3$  wt %. In the insets of Figure 9, and Figure 10, we observe that  $G'(\omega)$  does not vary too much along two or three orders of magnitude. In a log–log graph, the moduli depend linearly on the frequency with a small slope.

**3.3.3. Rheological Model for the SWCNTs/PAA Suspensions.** As mentioned, the intertube attraction in SWCNTs dispersed in

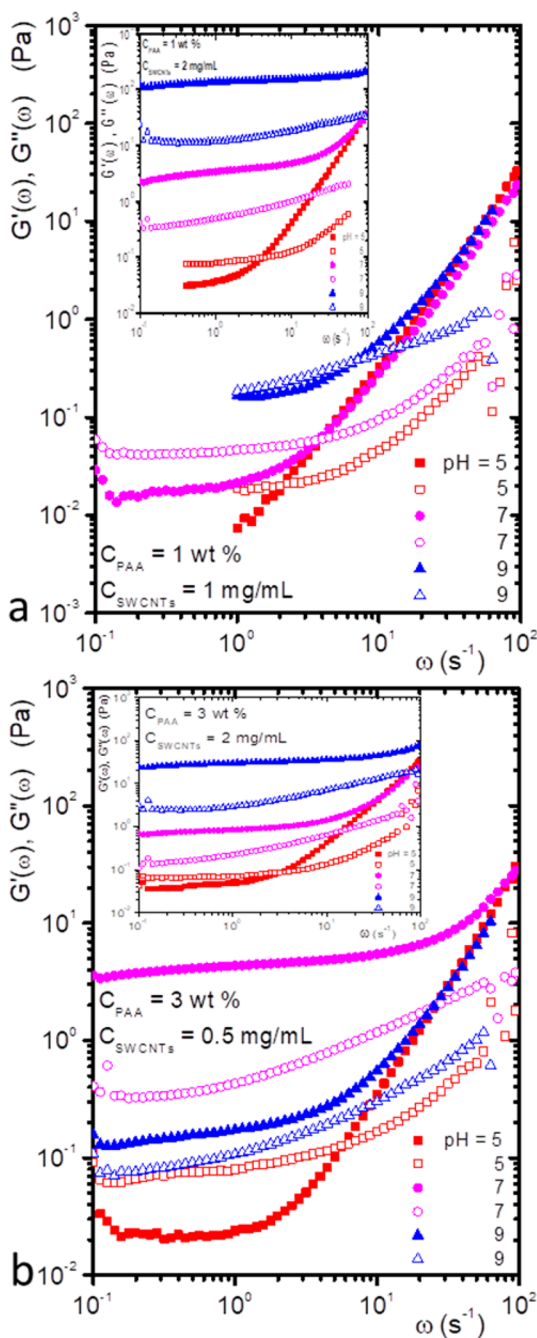


**Figure 9.** Viscoelastic spectra for SWCNTs/PAA water suspensions at different concentrations and pH. Closed symbols,  $G'(\omega)$ ; open symbols,  $G''(\omega)$ . (a)  $C_{\text{PAA}} = 1$  wt % and  $C_{\text{SWCNTs}} = 1$  mg/mL. Inset:  $C_{\text{PAA}} = 1$  wt % and  $C_{\text{SWCNTs}} = 2$  mg/mL. (b)  $C_{\text{PAA}} = 3$  wt % and  $C_{\text{SWCNTs}} = 0.5$  mg/mL. Inset:  $C_{\text{PAA}} = 3$  wt % and  $C_{\text{SWCNTs}} = 2$  mg/mL. pH = 5, 7, and 9.

polymers yields to the formation of aggregates or bundles even at a modest concentration. At the percolation concentration, a matrix spanning network must be formed that gives rise to elasticity, because nanotubes are arrested; as the number of nanotubes increases the elasticity of the composite increases. Around this percolation concentration, the rheological behavior must be dominated by that mesoscale superstructure. SEM and AFM surveys show that the SWCNTs/PAA suspensions presented a mesoscopic structure as pH reached high values. On the other hand, UV-vis spectra also indicate that exfoliated nanotubes, that is, individual entities or very thin bundles are

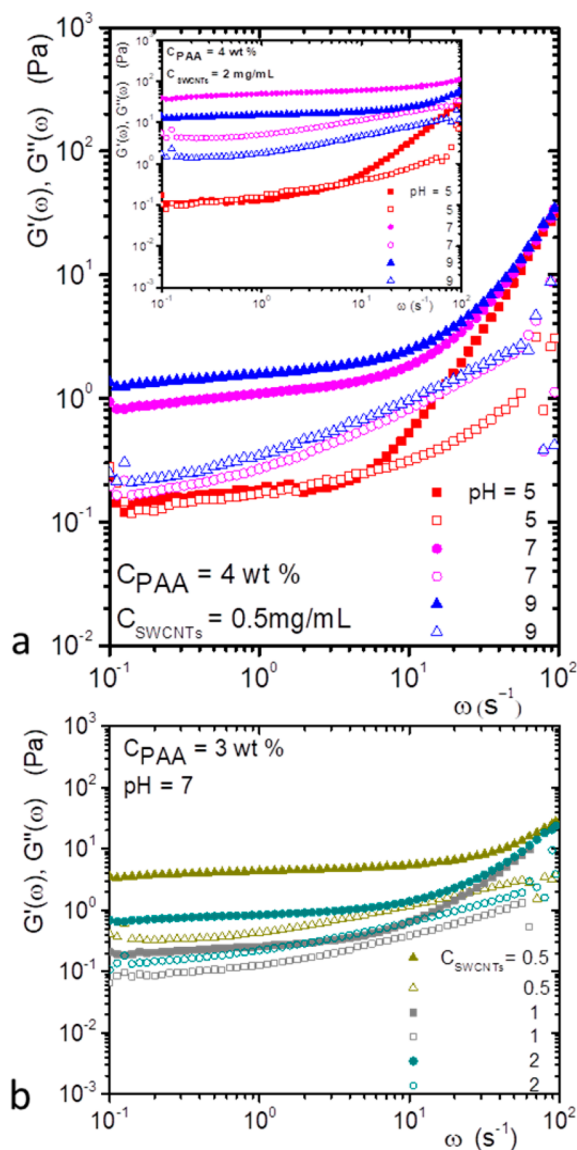


**Figure 10.** Viscoelastic spectra for SWCNTs/PAA water suspensions. Closed symbols,  $G'(\omega)$ ; open symbols,  $G''(\omega)$ : (a)  $C_{\text{PAA}} = 4$  wt % and  $C_{\text{SWCNTs}} = 0.5$  mg/mL. pH = 5, 7, and 9. (b)  $C_{\text{PAA}} = 3$  wt % and pH = 7 when the  $C_{\text{SWCNTs}}$  is varied.

present at low pH; but at high pH, they form bundles. Furthermore, viscoelastic spectra also show that the liquid-like viscoelastic behavior is lost in place of a solid-like at high pH values. Here, at  $\text{pH} \leq 5$ ,  $G''(\omega) > G'(\omega)$  at  $\omega < \omega_0$  and  $G''(\omega) < G'(\omega)$  at  $\omega > \omega_0$ ; when pH reaches a value  $> 5$ ,  $G'(\omega) \gg G''(\omega)$ . At high pH,  $\eta_0$  also grows to huge numbers as  $\dot{\gamma} \rightarrow 0$  similar to what occurs when a weak structure is formed within the fluid, which is quiescent at rest, but it does not resist deformation.

Cross-linking materials form molecular clusters that can grow in size. When the largest cluster diverges in size, at the percolation concentration, a transition from liquid to solid occurs. Materials at this transition or gel point are known as critical gels. In general, for critical gels, the long-range connectivity in the material can be reached by different mechanisms. In one named chemical gelation, permanent covalent bonds connect molecular strands into a three-dimensional network. In the other named physical gelation, bonds are temporary, of reversible nature, and the average

lifetime of such bonds are long compared with the observation time. Here, the system under study is behaving like a physical gel; the cross-linking is due to the attractive interaction that is tuned by pH. The overall interaction potential between the suspended CNTs stems from a balance between the van der Waals forces and the pH-sensitive charged moieties of the adsorbed polymeric layer on the tubes. Also, polymers in the polymeric layer can entangle with other polymers free or adsorbed in other polymeric layers. Winter and co-workers have characterized critical gels where dynamic arrest leads to gelation due to attractive interactions.<sup>28</sup>

Critical gels exhibit an unusually simple and regular relaxation behavior, which expresses itself in a self-similar relaxation modulus  $G(t) = St^{-n}$ , where  $G(t)$  is the real relaxation modulus,<sup>28</sup> and  $S$  and  $n$  are the two fitting material parameters that characterize the gel.  $S$  is the “strength” of the network, since it increases as the number of contacts or bonds between tubes;  $n$  reflects the nature of the size distribution of the mesoscale superstructure. A higher value of  $n$  means a broader aggregate size distribution, consistent with a slightly more open structure.<sup>36</sup> The values of  $n$  range between 0 and 1, and provide structural information. The power law implies that relaxation processes appear to be the same on all time scales. This model assumes that the gel does not exhibit a transition to glassy behavior. Thus, in the frequency domain, the power law behavior extends over all the frequencies,  $0 < \omega < \infty$ , because large frequencies are completely out of the range of measurements. Consequently, the time or frequency dependence of rheological properties is a simple power law. Close to the gel point,  $G'(\omega) = G'_c \omega^n$  and  $G''(\omega) = G''_c \omega^m$ , where  $G'_c$  and  $G''_c$  represent two material constants. Chambon and Winter<sup>27</sup> using the Kramers–Kronig relation found out that both exponents must be equal,  $n = m$ , and the relation between the material parameters is  $G'_c = G''_c / \tan(n\pi/2)$  in the range  $0 < n < 1$ . Then, the viscoelastic moduli are related as

$$\begin{aligned} G'(\omega) &= G''(\omega) / \tan(n\pi/2) \\ &= G'_c \omega^n = S \Gamma(1-n) \cos(n\pi/2) \omega^n \end{aligned} \quad (1)$$

Here,  $n < 1$ ,  $0 < \omega < \infty$ , and  $S = \frac{2\Gamma(n)}{\pi} \sin(n\pi/2) G'_c$ , where  $\Gamma(n)$  is the gamma function, and clearly  $G'' > G'$  for  $n > 1/2$ ,  $G' > G''$  for  $n < 1/2$ , and  $G' = G''$  for  $n = 1/2$ . To ensure that a system is around the gel point, using Flory’s principles ( $\eta_0 \rightarrow \infty$ , and  $G_{\infty} = 0$ )<sup>37</sup> is experimentally difficult.<sup>27,28</sup> A more general method to find the gel point in a system consists in the calculation of the tangent of the phase angle between the dynamical moduli,  $\tan \delta = G''(\omega) / G'(\omega)$ . When the tangent of the phase  $\delta$  is independent of the frequency, we can ensure that the system is in the gel point, and the value of  $n$  can be estimated directly,  $\tan \delta = \tan(n\pi/2)$ , for  $0 < n < 1$ . Since our suspensions apparently are forming a physical gel, we will use these arguments to find where they reach the gel point.

Figure 11 shows some examples of how the experimental measured  $\tan \delta = G''(\omega) / G'(\omega)$  depends on  $\omega$  for different  $C_{\text{PAA}}$  and  $C_{\text{SWCNTs}}$  when the pH is varied. We included the case of pure PAA just for contrasting the results obtained with the suspensions. In Figure 11a and its inset, we observe that  $\tan \delta$  for pure PAA is not a constant because it is far from forming a gel at these concentrations. However, when we add a small amount of SWCNTs (0.5 mg/mL) to the polymer ( $C_{\text{PAA}} = 2$  wt % or 3 wt %), the behavior of the curve  $\tan \delta$  vs  $\omega$  turns out to be completely different. For pH = 7 and pH = 9,  $\tan \delta$  is small but

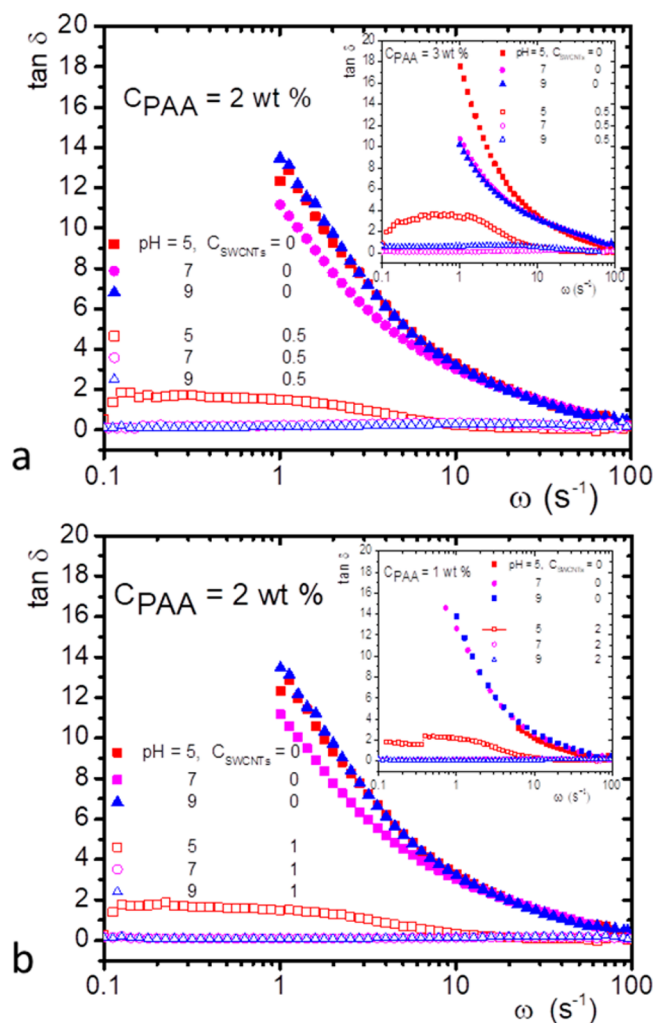


**Figure 11.**  $\tan \delta$  vs  $\omega$  for pure PAA (closed symbols) and SWCNTs/PAA suspensions (open symbols) as a function of pH. (a)  $C_{\text{PAA}} = 2$  wt % and  $C_{\text{SWCNTs}} = 0.5$  mg/mL. Inset:  $C_{\text{PAA}} = 3$  wt % and  $C_{\text{SWCNTs}} = 0.5$  mg/mL. (b)  $C_{\text{PAA}} = 2$  wt % and  $C_{\text{SWCNTs}} = 1$  mg/mL. Inset:  $C_{\text{PAA}} = 1$  wt % and  $C_{\text{SWCNTs}} = 2$  mg/mL. pH = 5, 7, and 9.

essentially constant along three orders of magnitude of  $\omega$ . For pH = 5,  $\tan \delta$  is small, but it is not a constant. Apparently, the system is close to gel point when  $\text{pH} \geq 7$ , at these concentrations. The same is observed when we increase  $C_{\text{SWCNTs}}$  as seen in Figure 11b ( $C_{\text{PAA}} = 2$  wt % and  $C_{\text{SWCNTs}} = 1$  mg/mL), or its inset for the case of  $C_{\text{PAA}} = 1$  wt % and  $C_{\text{SWCNTs}} = 2$  mg/mL; here it is possible to see that we are close to the gel point when  $\text{pH} > 5$ . However, lowering the concentration of CNTs,  $C_{\text{SWCNTs}} \leq 1$  mg/mL when  $C_{\text{PAA}} = 1$  wt %, we are not close to the gel point because  $\tan \delta$  as a function of  $\omega$  is not a constant even at  $\text{pH} > 5$  (not shown). Several combinations of  $C_{\text{PAA}}$  up to 6 wt % and CNTs present a similar pattern (not shown).

Depending on how good the system behaves as the proposed model,  $n$  will be a constant that does not depend on the frequency at the gel point. The suspensions that present less variation in the experimental  $\tan \delta$  vs  $\omega$  plots were used to calculate the best horizontal line fit along three orders of magnitude in  $\omega$  to give the exponent  $n$ , using  $\tan \delta = \tan(n\pi/2)$ . Predictions of the moduli were made using  $G'(\omega) = G'_c \omega^n$  and  $G''(\omega) = G''_c \omega^n$ , where the fitting parameters  $S$ ,  $G'_c$ , and  $G''_c$  were obtained (eq 1). Figure 12 presents the predicted and experimental moduli for those cases very close to the gel point

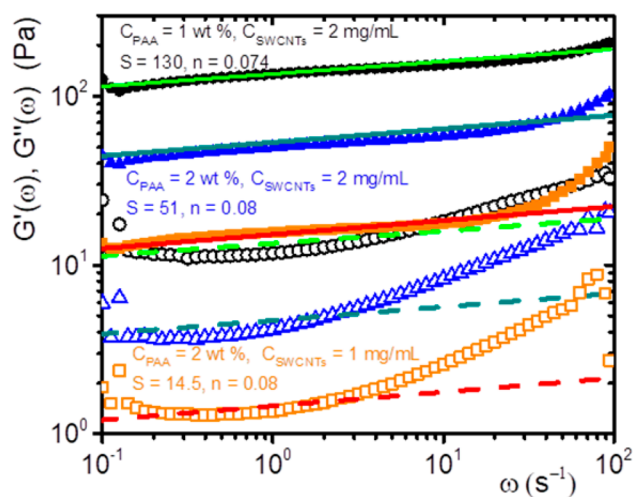


**Figure 12.** Predicted and experimental shear moduli ( $G'(\omega)$  closed symbols  $G''(\omega)$  open symbols) for three cases closer to the gel point as a function of the frequency that turned out to be at pH = 9. Straight lines correspond to model  $G'(\omega) = G'_c \omega^n$  and dashed lines correspond to  $G''(\omega) = G''_c \omega^n$ .

that turned out to be the suspensions with pH = 9 for  $C_{\text{PAA}} = 1$  wt % and  $C_{\text{SWCNTs}} = 2$  mg/mL. Here, the prediction of  $G'(\omega)$  is excellent and for  $G''(\omega)$  is reasonable for 2 orders of magnitude in  $\omega$ ; the parameters are given in the figure. The same occurs for the case of  $C_{\text{PAA}} = 2$  wt %, but here the gel point seems to be closer when  $C_{\text{SWCNTs}} = 2$  mg/mL than when  $C_{\text{SWCNTs}} = 1$  mg/mL, both at pH = 9. As expected, the  $S$  value is higher for  $C_{\text{SWCNTs}} = 2$  mg/mL indicating that the number of contacts between nanotubes is larger, and as a consequence more elastic. On the other hand for  $C_{\text{SWCNTs}} = 1$  mg/mL, although  $S$  is still large, elasticity is lower than before. The experimental  $n$  values we found are small ( $n = 0.07$ – $0.08$ ), but relatively close to those found in other physical gels for instance, thermoplastic elastomeric polypropylene ( $n = 0.13$ – $0.18$ ),<sup>38</sup> and fd virus-PNIPAM ( $n = 0.08$ – $0.130$ ).<sup>36</sup> For physical gels,  $n$  values are usually much smaller than those for chemical gels that usually are larger than 0.5, revealing that the size distribution of the mesoscale superstructure is not as open as in the chemical gels. Therefore, we consider that our results for the system of interest here are in agreement with those of physical gels close to the gel point.

The gel of SWCNTs/PAA can be visualized by a cartoon given in Figure 13 that summarizes all our findings. In the suspension at pH = 5, CNTs are exfoliated and dispersed by the almost neutral coil-like polymer molecules adsorbed on them, as determined by the UV–vis spectrum. The contacts between CNTs are mainly through polymer entangling, and the suspension is viscoelastic. As pH increases, the polymer is charged, and the solution is not such a good solvent for the CNTs (pH > 5). Here, bundles are formed, and at some point, they mechanically percolate along the fluid and become arrested. As a consequence, the rheological behavior must be dominated by the formed mesoscale superstructure. In particular, viscoelasticity is lost, and the suspension becomes more elastic. At even higher pH, the surroundings for CNTs are worse, and bundles grow to a larger extent as determined by UV–vis, up to the point that they can be observable by SEM and AFM. In particular mixtures, the suspension reaches the gel point, where a power law can model the relaxation moduli in the frequency domain. In this suspension, pH can tune the gel formation making the solvent

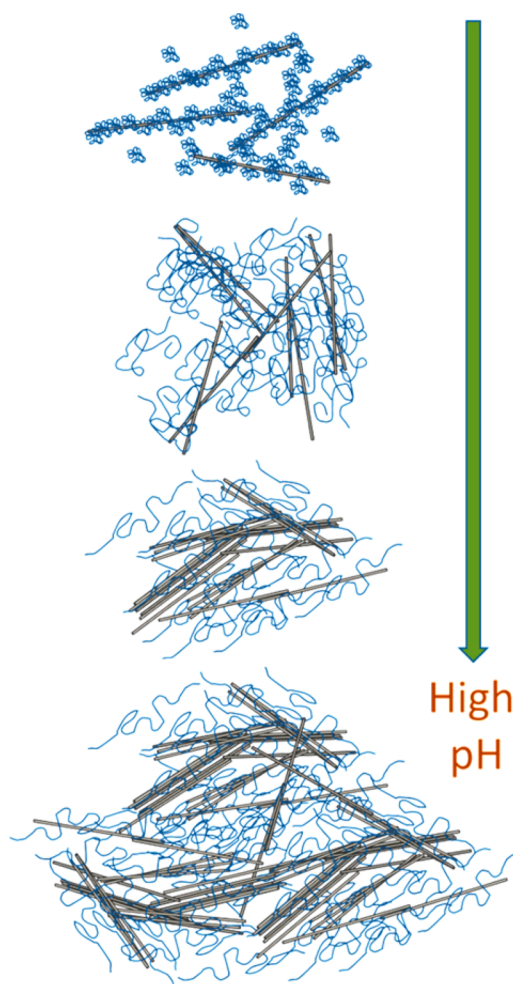


**Figure 13.** Schematics of the structure of SWCNTs/PAA suspensions as pH increases from low pH (top) to high pH (bottom).

less attractive to the CNTs, so they prefer to form interconnected bundles and flocs at low concentration. If we calculate in our suspensions the volume fraction ( $1 \times 10^{-4}$  to  $8 \times 10^{-4}$ ) and aspect ratio of SWCNTs ( $10^3$ ), we can localize our system in the holistic picture of geometric packing limits as reported in ref 1 for a broad range of rod microstructures for which elasticity has been measured. The suspensions are located in a region where CNT rods are not sufficiently crowded to arrest due to excluded volume interactions alone; however, attractive interactions between them are required to form a connected structure. Then, in this map, the resultant heterogeneous structures may be fractals or bundles. We suspect that our nanotube mesoscale superstructure dispersed in the polymer is made by heterogeneous rod fractal clusters. More research is needed to get more insight of the structure of these dark suspensions, although the size of the SWCNTs poses a problem for SANS or SAXS in the range of  $qL \sim 1$ .

#### 4. CONCLUSIONS

The shear viscosity and viscoelastic spectra were measured for both water solutions of poly(acrylic acid) without and with dispersed single-wall carbon nanotubes, around the overlap concentration of the polymer, at different pH values. In the former case, the polyelectrolyte is charged as pH increases, and due to the electrostatic repulsion between charged not protonated carboxyl groups, extended polymer structures are

formed exhibiting a viscoelastic rheological behavior. However, the crossing points collapse in a single exponential curve no matter the concentration and pH as mentioned in Figure 4b; as far as we know, it has not been observed before and it deserves further investigation to understand this fact. In the latter case, small quantities of SWCNTs were dispersed in the polyelectrolyte, making this study one of the very few focusing on the dilute regime rheology of CNTs dispersed in a polymer matrix. At low pH, the nanotube bundles exfoliate making it possible to embed the nanotubes as individual entities or as very thin bundles into the polymer matrix. As pH increases, the added nanotubes apparently form bundles surrounded by a polymer forming a weak mesoscopic network; this occurs at low poly(acrylic acid) and carbon nanotubes concentrations, where the suspensions are highly viscous at very low shear rates and shear thin dramatically at high shear rates. At a very low concentration of carbon nanotubes and for  $\text{pH} > 5$ , at the percolation concentration, the matrix spanning network increases elasticity because the CNTs are arrested. The suspensions lose their viscoelasticity, up to a point to lose the crossing points between the  $G'(\omega)$  and  $G''(\omega)$  curves.

At a very low concentration of carbon nanotubes and polymer ( $\leq C^*$ ), due to the presence of the mesoscale superstructure formed by nanotubes and polymer, we found that the system behaves as a critical gel. For the first time, as far as we know, it was noticed that close to the gel point these suspensions exhibit a self-similar relaxation modulus ( $G(t) = St^{-n}$  or as a power law  $G^*(\omega) \propto \omega^n$  in the frequency domain) where pH is the tuning parameter between viscoelasticity and solid gel behavior. The exponent values were evaluated for a couple of suspensions close to their gel points. The power law relaxation moduli description is excellent, for three and two orders of magnitude in  $\omega$  for  $G'(\omega)$  and  $G''(\omega)$ , respectively. However, the bonds maintaining the gel structure are soft, as in physically interconnected solid gels, because the system can flow when shear is applied to the suspension. We suspect that our mesoscale superstructure formed by nanotubes in the polymer is made of heterogeneous rod fractal clusters. Further studies are underway.

## AUTHOR INFORMATION

### Corresponding Author

\*E-mail: [rolandoc@fisica.unam.mx](mailto:rolandoc@fisica.unam.mx).

### ORCID

Antonio Tavera-Vázquez: 0000-0001-8304-2123

Rolando Castillo: 0000-0001-6331-0311

### Author Contributions

#A.S. and A.T.-V. contributed equally to this work.

### Notes

The authors declare no competing financial interest.

## ACKNOWLEDGMENTS

Financial support from SEP-CONACyT (Inf 280010, and FC 076), and DGAPA-UNAM (IN 106218) are gratefully acknowledged. We also thank Dr. S. Tehuacanero-Cuapa and Dr. D. Montalvan for their help to get the SEM and TEM images, respectively, and to Dr. M. Quintana from IFUASLP for her helpful discussion.

## REFERENCES

(1) Solomon, M. J.; Spicer, P. T. Microstructural Regimes of Colloidal Rod Suspensions, Gels, and Glasses. *Soft Matter* **2010**, *6*, 1391–1400.

(2) Dresselhaus, M. S.; Dresselhaus, G.; Avouris, P., Eds. *Carbon Nanotubes: Synthesis, Structure, Properties and Applications*; Springer-Verlag: Heidelberg, 2001.

(3) Baughman, R. H.; Zakhidov, A. A.; de Heer, W. A. Carbon Nanotubes. The Route Toward Applications. *Science* **2017**, *297*, 787–792.

(4) Israelachvili, J. *Intermolecular & Surface Forces*, 2nd ed.; Academic Press: London, 1992.

(5) Manivannan, S.; Jeong, I. O.; Ryu, J. H.; Lee, C. S.; Kim, K. S.; Jang, J.; Park, K. C. Dispersion of Single-Walled Carbon Nanotubes in Aqueous and Organic Solvents Through a Polymer Wrapping Functionalization. *J. Mater. Sci.: Mater. Electron.* **2009**, *20*, 223–229.

(6) Huang, Y. Y.; Terentjev, E. M. Dispersion of Carbon Nanotubes: Mixing, Sonication, Stabilization, and Composite Properties. *Polymers* **2012**, *4*, 275–295.

(7) Saint-Aubin, K.; Poulin, P.; Saadaoui, H.; Maugey, M.; Zakri, C. Z. Dispersion and Film-Forming Properties of Poly(acrylic acid)-Stabilized Carbon Nanotubes. *Langmuir* **2009**, *25*, 13206–13211.

(8) Ayewah, D. O. O.; Davis, D. C.; Krishnamoorti, R.; Lagoudas, C. D.; Sue, H. J.; Willson, M. A. Surfactant Dispersed SWCNT-Polystyrene Composite Characterized for Electrical and Mechanical Properties. *Composites, Part A* **2010**, *41*, 842–849.

(9) O'Connell, M. J.; Boul, P.; Ericson, L. M.; Huffman, C.; Wang, Y.; Haroz, E.; Kuper, C.; Tour, J.; Ausman, K. D.; Smalley, R. E. Reversible Water-Solubilization of Single-Walled Carbon Nanotubes by Polymer Wrapping. *Chem. Phys. Lett.* **2001**, *342*, 265–271.

(10) Chatterjee, T.; Yurekli, K.; Hadjiev, V. G.; Krishnamoorti, R. Single-Walled Carbon Nanotube Dispersion in Poly(ethylene oxide). *Adv. Funct. Mater.* **2005**, *15*, 1832–1838.

(11) Rouse, J. H.; Lillehei, P. T. Electrostatic Assembly of Polymer/Single Walled Carbon Nanotube Multilayer Films. *Nano Lett.* **2003**, *3*, 59–62.

(12) Chen, R. J.; Zhang, Y.; Wang, D.; Dai, H. Noncovalent Sidewall Functionalization of Single-Walled Carbon Nanotubes for Protein Immobilization. *J. Am. Chem. Soc.* **2001**, *123*, 3838–3839.

(13) Bahr, J. L.; Yang, J. P.; Kosynkin, D. V.; Bronikowski, M. J.; Smalley, R. E.; Tour, J. M. Functionalization of Carbon Nanotubes by Electrochemical Reduction of Aryl Diazonium Salts: A Bucky Paper Electrode. *J. Am. Chem. Soc.* **2001**, *123*, 6536–6542.

(14) Sun, Y.; Wilson, S. R.; Schuster, D. I. High Resolution and Strong Light Emission of Carbon Nanotubes in Aromatic Amine Solvents. *J. Am. Chem. Soc.* **2001**, *123*, 5348–5349.

(15) Mickelson, E. T.; Huffman, C. B.; Rinzler, A. G.; Smalley, R. E.; Hauge, R. H.; Margrave, J. L. Fluorination of Single-Wall Carbon Nanotubes. *Chem. Phys. Lett.* **1998**, *296*, 188–194.

(16) Georgakilas, V.; Kordatos, K.; Prato, M.; Guldi, D. M.; Holzinger, M.; Hirsch, A. Organic Functionalization of Carbon Nanotubes. *J. Am. Chem. Soc.* **2002**, *124*, 760–761.

(17) Sohrabi, B.; Poorgholami-Bejarpasi, N.; Nayeri, N. Dispersion of Carbon Nanotubes Using Mixed Surfactants: Experimental and Molecular Dynamics Simulation Studies. *J. Phys. Chem. B* **2014**, *118*, 3094–3103.

(18) Chen, D. T. N.; Chen, K.; Hough, L. A.; Islam, M. F.; Yodh, A. G. Rheology of Carbon Nanotube Networks During Gelation. *Macromolecules* **2010**, *43*, 2048–2053.

(19) Shin, J. Y.; Premkumar, T.; Geckeler, K. E. Dispersion of Single-Walled Carbon Nanotubes by Using Surfactants: Are the Type and Concentration Important? *Chem. - Eur. J.* **2008**, *14*, 6044–6048.

(20) Brunecker, F. K.; Schöppler, F.; Hertel, T. Interaction of Polymers with Single-Wall Carbon Nanotubes. *J. Phys. Chem. C* **2016**, *120*, 10094–10103.

(21) Lin, Y.; Allard, L. F.; Sun, Y. P. Protein-Affinity of Single-Walled Carbon Nanotubes in Water. *J. Phys. Chem. B* **2004**, *108*, 3760–3764.

(22) Chatterjee, T.; Krishnamoorti, R. Rheology of Polymer Carbon Nanotubes Composites. *Soft Matter* **2013**, *9*, 9515–9529.

(23) Davis, V. A.; Parra-Vasquez, A. N.; Green, M. J.; Rai, P. K.; Behabtu, N.; Prieto, V.; Booker, R. D.; Schmidt, J.; Kesselman, E.; Zhou, W.; et al. True Solutions of Single-Walled Carbon Nanotubes for

Assembly into Macroscopic Materials. *Nat. Nanotechnol.* **2009**, *4*, 830–834.

(24) Dobrynin, A. V.; Rubinstein, M. Theory of Polyelectrolytes in Solutions and at Surfaces. *Prog. Polym. Sci.* **2005**, *30*, 1049–1118.

(25) Sharma, A.; Smith, J. D.; Walters, K. B.; Rick, S. W. Constant pH Simulations of pH Responsive Polymers. *J. Chem. Phys.* **2016**, *145*, 234906.

(26) Swift, T.; Swanson, L.; Geoghegan, M.; Rimmer, S. The pH-responsive Behaviour of Poly(acrylic acid) in Aqueous Solution is Dependent on Molar Mass. *Soft Matter* **2016**, *12*, 2542–2549.

(27) Chambon, F.; Winter, H. H. Linear Viscoelasticity at the Gel Point of a Crosslinking PDMS with Imbalanced Stoichiometry. *J. Rheol.* **1987**, *31*, 683–697.

(28) Schwittay, C.; Mours, M.; Winter, H. H. Rheological Expression of Physical Gelation in Polymers. *Faraday Discuss.* **1995**, *101*, 93–104.

(29) Asahina, S.; Togashi, T.; Terasaki, O.; Takam, S.; Adschiri, T.; Shibata, M.; Erdman, N. High-Resolution Low-Voltage Scanning Electron Microscope Study of Nanostructured Materials. *Microsc. Anal.* **2012**, *26*, S12–S14.

(30) Rubinstein, M.; Colby, R. H. *Polymer Physics*; Oxford, U.K., 2003.

(31) Etika, K. C.; Cox, M. A.; Grunlan, J. C. Tailored Dispersion of Carbon Nanotubes in Water with pH-Responsive Polymers. *Polymer* **2010**, *51*, 1761–1770.

(32) Grossiord, N.; Loos, J.; Meuldijk, J.; Regev, O.; Miltner, H. E.; Mele, B. V.; Koning, C. E. Conductive Carbon-Nanotube/Polymer Composites: Spectroscopic Monitoring of the Exfoliation Process in Water. *Compos. Sci. Technol.* **2007**, *67*, 778–782.

(33) Kuwahara, S.; Sugai, T.; Shinohara, H. Determining Exact Molar Absorbance Coefficients of Single-Wall Carbon Nanotubes. *Phys. Chem. Chem. Phys.* **2009**, *11*, 1091–1097.

(34) Lenstra, T. A. J.; Dogic, Z.; Dhont, J. K. G. Shear-Induced Displacement of Isotropic-Nematic Spinodals. *J. Chem. Phys.* **2001**, *114*, 10151–10162.

(35) Raghavan, S. R.; Douglas, J. F. The Conundrum of Gel Formation by Molecular Nanofibers, Wormlike Micelles, and Filamentous Proteins: Gelation without Cross-Links? *Soft Matter* **2012**, *8*, 8539–8546.

(36) Reddy, N. K.; Zhang, Z.; Lettinga, M. P.; Dhont, J. K. G.; Vermant, J. Probing Structure in Colloidal Gels of Thermoreversible Rodlike Virus Particles: Rheology and Scattering. *J. Rheol.* **2012**, *56*, 1153–1174.

(37) Flory, P. J. *Principles of Polymer Chemistry*; Cornell University Press: Ithaca, NY, 1953.

(38) Lin, Y. G.; Mallin, D. T.; Chien, J. C. W.; Winter, H. H. Dynamic Mechanical Measurement of Crystallization-Induced Gelation in Thermoplastic Elastomeric Poly(propylene). *Macromolecules* **1991**, *24*, 850–854.